Automated Breast Mass Segmentation using Pulse-Coupled Neural Network and Distance Regularized Level Set Evolution: A Coarse-to-fine Approach

Songlin Du, Yaping Yan and Yide Ma
School of Information Science and Engineering, Lanzhou University, Lanzhou, 730000, China

Keywords: Breast Mass Segmentation, Pulse-Coupled Neural Network, Distance Regularized Level Set Evolution.

Abstract: *Motivation*: Computer-aided diagnosis (CAD) is an important means for the clinical detection of breast cancer. Mass is a common manifestation of breast cancer. This work aims to develop an effective breast mass segmentation algorithm for CAD systems. *Method*: On one hand, pulse-coupled neural network (PCNN) and level set (LS) method have complementary advantages in image segmentation, we therefore combine PCNN and LS. On the other hand, traditional LS method formulates the evolution of the contour through the evolution of a level set function (LSF), and LSF typically develops irregularities during its evolution, which may cause numerical errors and eventually destroy the stability of the evolution. So we use an improved LS model, named distance regularized level set evolution (DRLSE), to achieve desirable segmentation performance. Specifically, we extract the region of interest (ROI) with PCNN and sets initial contour for DRLSE first. Then the finely segmentation is achieved by DRLSE. *Results*: Both qualitative and quantitative experiments on three large-scale mammography databases prove that the proposed method achieves high segmentation accuracy. *Conclusion*: The proposed algorithm is effective for automatic breast mass segmentation. *Significance*: First, the sketchy position of mass is fixed by PCNN, which guides the algorithm to define a flexibly initial contour for DRLSE. This strategy makes it easier for the contour to move from initial position towards the boundary between mass and normal tissue. Second, the use of DRLSE, which introduces an intrinsic capability of maintaining regularity of the LSF, ensures stable LS evolution and achieves accurate segmentation.

1 INTRODUCTION

1.1 Background and Motivation

Breast cancer is one of the most common cancers among women, and the key action to reduce the death rate due to breast cancer is early detection (Liang et al., 2012). Mammography screening, which is a specific technique of imaging that uses a low-dose X-ray system and high-contrast, high-resolution film for breast examination, can depict most of the significant abnormal tissues in breast. Computer-aided diagnosis (CAD) techniques in mammography serve as a second opinion for radiologists by identifying regions with high suspicion of malignancy (Astley, 2004). Breast mass is a common manifestation of breast cancer that continues to challenge both radiologists and CAD systems (Eltonsy et al., 2007; Guo et al., 2015). However, accurate detection of breast mass is challenging for its complex topological structures and heterogeneous intensity distributions (Cui et al., 2009). The task of breast mass detection is essentially a problem of image segmentation. Image segmentation studies how to partition an image into several meaningful parts, often consisting of objects and backgrounds (Zhang and Ji, 2011; Du et al., 2014). As an important technique in many computer vision related applications, it is of general interest to design robust and fast segmentation algorithms. However, it is widely accepted that there is no general method for solving all segmentation problems. On the contrary, to achieve satisfactory performances, algorithms should be highly adapted to their corresponding applications. In recent years, plenty of image segmentation algorithms which were developed in the field of computer vision have been introduced to the detection and the segmentation of breast lesions. For example, Z. Wang *et al.* (Wang et al., 2014) proposed to combine wavelet modulus maxima transform, morphological operation, and region grow for breast tumor edge segmentation. L. Moraru *et al.* (Moraru et al., 2014) transferred the problem

Du, S., Yan, Y. and Ma, Y.
Automated Breast Mass Segmentation using Pulse-Coupled Neural Network and Distance Regularized Level Set Evolution: A Coarse-to-fine Approach.
DOI: 10.5220/0005621300170024
In *Proceedings of the 9th International Joint Conference on Biomedical Engineering Systems and Technologies (BIOSTEC 2016) - Volume 2: BIOIMAGING*, pages 17-24
ISBN: 978-989-758-170-0

of breast lesion segmentation into extracting texture features. R. Rouhi *et al.* (Rouhi et al., 2015) employed region growing and cellular neural network (CNN) segmentation for benign and malignant breast tumors classification. W. Xie *et al.* (Xie et al., 2016) employed level set and extreme learning machine for breast mass classification. In this paper, we studied the problem of partitioning breast mass in mammography, and proposed a coarse-to-fine method which combines pulse-coupled neural network (PCNN) and distance regularized level set evolution (DRLSE).

1.2 Our Contribution

The PCNN, which has fundamental advantages in image processing because of its biological background, was constructed by R. Eckhorn *et al.* (Eckhorn et al., 1989; Eckhorn et al., 1990) to simulate the synchronous pulse bursts in cat visual cortex. Thus far, a large plenty of literatures aiming at the applications of PCNN have been published, such as image segmentation (Kuntimad and Ranganath, 1999), image fusion (Li et al., 2006), and edge detection (Zhou et al., 2008). However, the strength of PCNN lies in finding sketchy positions of homogeneous regions in natural images, and it is hard for PCNN to position boundaries between different regions precisely. On the contrary, by minimizing an energy functional, the level set (LS) method, which was proposed by S. Osher and J. A. Sethian (Osher and Sethian, 1988), is able to achieve accurate detection of the edges of homogeneous regions on condition that the sketchy positions of the homogeneous regions are known. Therefore, we deem that PCNN and LS have complementary advantages in image segmentation. In our previous work, W. Xie *et al.* (Xie et al., 2015) propose to combine PCNN and traditional LS to achieve breast mass segmentation. However, traditional LS methods represent a contour or interface as the zero level set of a level set function (LSF), and formulate the evolution of the contour through the evolution of the LSF, which typically develops irregularities during its evolution, may cause numerical errors and eventually destroy the stability of the evolution (Li et al., 2010). We therefore use the DRLSE (Li et al., 2010), which is an improved LS model, instead of using traditional LS methods. Specifically, the proposed strategy employs PCNN to fix the sketchy position of mass by coarsely segmentation. After that, based on the coarsely segmentation result of PCNN, some basic geometric methods are used to set initial contour for DRLSE automatically. At last, the task of finely segmentation is carried out by DRLSE. Experimental results on three mammography databases tell that the segmentation results are very close to the ground-truth, which prove the accuracy of the proposed method.

2 RELATED WORKS

The definitions and principles of PCNN and DRLSE are successively reviewed and analyzed in the reminder of this section.

2.1 Pulse-Coupled Neural Network

As mentioned above, PCNN was proposed to simulate synchronous pulse bursts in cat visual cortex. Therefore, compared with traditional artificial neural networks, the bio-inspired neuron model of PCNN is more sophisticated. As illustrated in Figure 1, neuron model of PCNN consists of three parts, i.e., input part, linking part, and pulse generator part (Wang et al., 2010). The neuron receives information from input signal and neighborhood neurons through input part, these two kinds of information are linked by the linking part, then the pulse generator part generates pulses as outputs of the neuron.

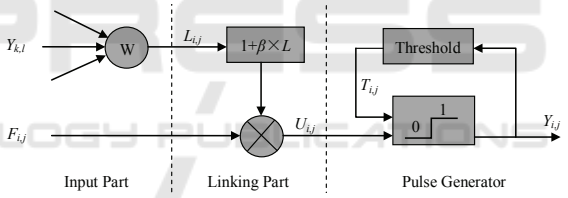

Figure 1: Neuron model of PCNN.

In image processing, pixels of the input image should be mapped into neurons in PCNN. The neuron model which is presented in Figure 1 can be quantitatively described as iteration by (Eckhorn et al., 1989; Eckhorn et al., 1990; Wang et al., 2010)

$$F_{i,j}[n] = e^{-\alpha_F} F_{i,j}[n-1] + V_F \sum_{k,l} w_{i,j,k,l} Y_{k,l}[n-1] + S_{i,j}, \quad (1)$$

$$L_{i,j}[n] = e^{-\alpha_L} L_{i,j}[n-1] + V_L \sum_{k,l} m_{i,j,k,l} Y_{k,l}[n-1], \quad (2)$$

$$U_{i,j}[n] = F_{i,j}[n](1+\beta L_{i,j}[n]), \quad (3)$$

$$T_{i,j}[n] = e^{-\alpha_T} T_{i,j}[n-1] + V_T Y_{i,j}[n], \quad (4)$$

$$Y_{i,j}[n] = \begin{cases} 1, & U_{i,j}[n] > T_{i,j}[n] \\ 0, & \text{otherwise} \end{cases}, \quad (5)$$

where (i, j) is the coordinates of the pixel which is corresponding to the current neuron. n denotes iteration steps. $S_{i,j}$ is the input signal, i.e., gray-level value

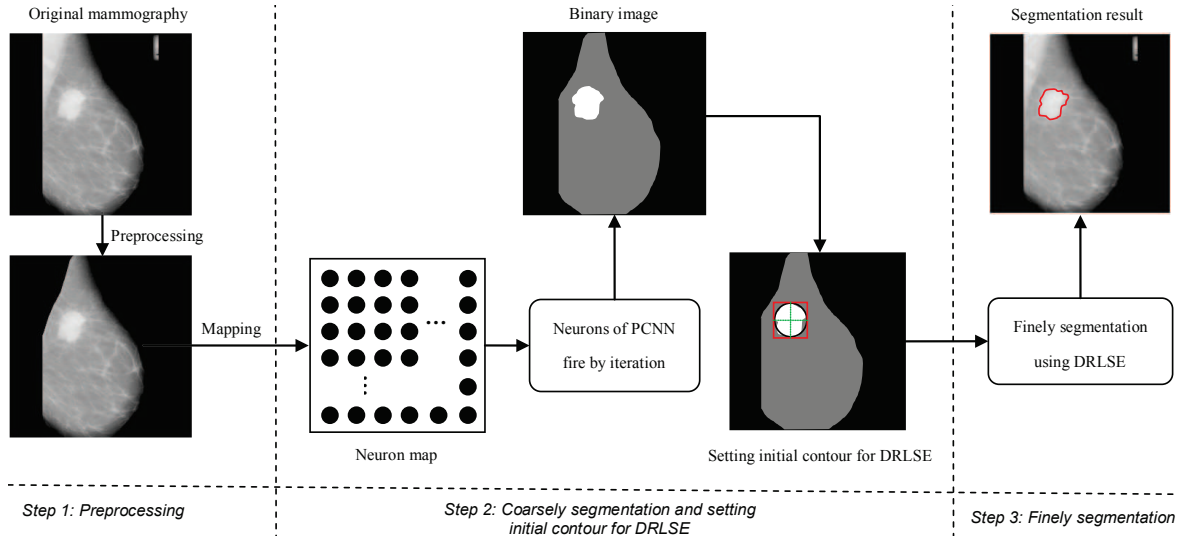

Figure 2: A graphical illustration of the proposed method.

of the current pixel. $F_{i,j}$ and $L_{i,j}$ are feedback input and linking input of the current neuron. $w_{i,j,k,l}$ and $m_{i,j,k,l}$ are constant synaptic weight matrices for feeding and linking inputs, respectively, which depends on the distance between the current neuron (i,j) and its neighbourhood neuron (k,l). $F_{i,j}$ and $L_{i,j}$ are modulated through a linking strength β. $U_{i,j}$, which is named as internal activity, is the modulating result of $F_{i,j}$ and $L_{i,j}$. $T_{i,j}$ is a dynamic threshold which decays by coefficients α_T while the current neuron is not yet fired. The neuron generates a pulse to $Y_{i,j}$ while the internal activity $U_{i,j}$ is greater than the dynamic threshold $T_{i,j}$, otherwise, it remains quiet. In other words, $Y_{i,j}$ is the output of the current neuron. V_F, V_L, and V_T are initial amplitudes of $F_{i,j}$, $L_{i,j}$, and $T_{i,j}$, respectively. α_F and α_L are decaying coefficients of $F_{i,j}$ and $L_{i,j}$, respectively.

2.2 Distance Regularized Level Set Evolution

As mentioned above, the LS method represents a contour or interface as the zero level set of a LSF, and formulates the evolution of the contour through the evolution of the LSF (Estellers et al., 2012). However, traditional LSF typically develops irregularities during its evolution, which may cause numerical errors and eventually destroy the stability of the evolution (Li et al., 2010). To solve this problem, C. Li *et al.* (Li et al., 2010) constructed a new type of LS evolution, which ia abbreviated DRLSE, by defining an energy functional $\varepsilon(\phi)$ by (Li et al., 2010)

$$\varepsilon(\phi) = \mu\mathcal{R}_p(\phi) + \varepsilon_{\text{ext}}(\phi), \tag{6}$$

where μ is a positive constant, $\varepsilon_{\text{ext}}(\phi)$ is an external energy term, and $\mathcal{R}_p(\phi)$ is the level set regularization term defined by (Li et al., 2010)

$$\mathcal{R}_p(\phi) \triangleq \int_\Omega p(|\nabla\phi|)\,dx, \tag{7}$$

where p is an energy density function $p:[0,\infty)\to\Re$.

In image segmentation applications, an edge indicator function g can be defined by (Li et al., 2010)

$$g \triangleq \frac{1}{1+|\nabla G_\sigma * I|^2}, \tag{8}$$

where G_σ is a Gaussian kernel with a standard deviation σ. For a LSF $\phi:\Omega\to\Re$, the line integral of the function g along the zero level contour of ϕ can be calculated with the Dirac delta function δ as

$$\mathcal{L}_g(\phi) \triangleq \int_\Omega g\delta(\phi)|\nabla\phi|\,dx, \tag{9}$$

and a weighted area of the region $\Omega_\phi^- \triangleq \{x:\phi(x)<0\}$ can be calculated with the Heaviside function H as (Li et al., 2010)

$$\mathcal{A}_g(\phi) \triangleq \int_\Omega gH(-\phi)\,dx. \tag{10}$$

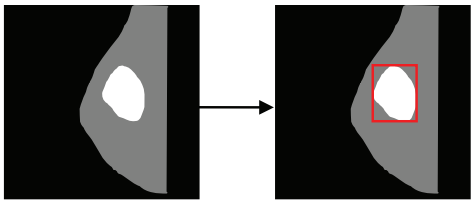

Figure 3: Schematic diagram of defining initial contour for DRLSE.

Then the energy functional $\varepsilon(\phi)$, i.e., (6), can be achieved by (Li et al., 2010)

$$\varepsilon(\phi) = \mu R_p(\phi) + \lambda \mathcal{L}_g(\phi) + \alpha \mathcal{A}_g(\phi), \quad (11)$$

where λ and α, which are subject to $\lambda > 0$ and $\alpha \in \Re$, are the coefficients of the energy functionals $\mathcal{L}_g(\phi)$ and $\mathcal{A}_g(\phi)$, respectively. In practice, the Dirac delta function δ and the Heaviside function H can be approximated by smooth functions δ_ε and the Heaviside function H_ε, which are defined by (Li et al., 2010)

$$\delta_\varepsilon(x) = \begin{cases} \frac{1}{2\varepsilon}\left[1+\cos\left(\frac{\pi x}{\varepsilon}\right)\right], & |x| \le \varepsilon \\ 0, & |x| > \varepsilon \end{cases} \quad (12)$$

and

$$H_\varepsilon(x) = \begin{cases} \frac{1}{2}\left[1+\frac{x}{\varepsilon}+\frac{1}{\pi}\sin\left(\frac{\pi x}{\varepsilon}\right)\right], & |x| \le \varepsilon \\ 1, & |x| > \varepsilon \\ 0, & |x| < -\varepsilon \end{cases}, \quad (13)$$

respectively. By replacing δ and H with (12) and (13) respectively, we can achieve the energy functional $\varepsilon(\phi)$ by (Li et al., 2010)

$$\begin{aligned} \varepsilon_\varepsilon(\phi) =& \mu \int_\Omega p(|\nabla\phi|)\,dx + \lambda \int_\Omega g\delta(\phi)|\nabla\phi|\,dx \\ &+ \alpha \int_\Omega gH(-\phi)\,dx. \end{aligned} \quad (14)$$

Given an initial LSF $\phi(x,0) = \phi_0(x)$, the approximated energy functional (14) can be minimized by solving (Li et al., 2010)

$$\begin{aligned} \frac{\partial\phi}{\partial t} =& \mu \mathrm{div}(d_p(|\nabla\phi|)|\nabla\phi|) \\ &+ \lambda\delta_\varepsilon(\phi)\,\mathrm{div}\left(g\frac{\nabla\phi}{|\nabla\phi|}\right) + \alpha g\delta_\varepsilon(\phi). \end{aligned} \quad (15)$$

3 THE PROPOSED BREAST MASS SEGMENTATION METHOD

The framework of the proposed method, which consists of three steps, is graphically illustrated in Figure 2. The first step is pre-processing, which removes tags, camera windows, and pectoral muscles from the original mammography. The second step conducts coarsely segmentation and sets initial contour for DRLSE. The last step achieves finely segmentation by using DRLSE. From another angle, the procedure of coarsely segmentation can be regarded as extracting the region of interest (ROI) from mammography. Since our method firstly extracts ROI with PCNN and then performs finely segmentation with DRLSE, we define it as a 'coarse-to-fine' strategy.

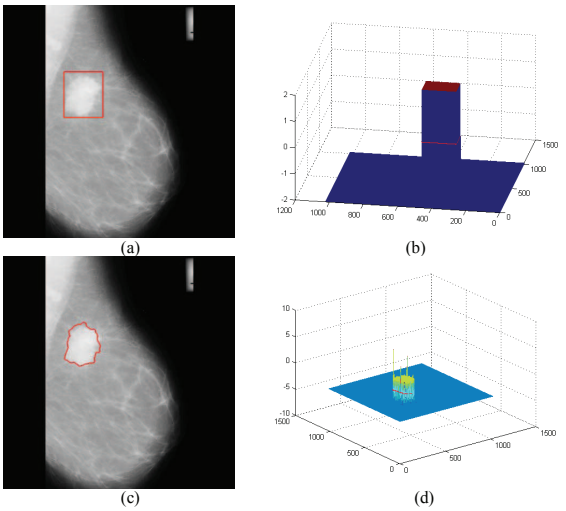

Figure 4: Visualization of the LSFs before and after evolution. (a) Initial contour. (b) Initial LSF. (c) Final contour. (d) Final LSF.

3.1 Coarsely Segmentation with PCNN

In the field of CAD, a ROI usually denotes a region which provides the rough location of a lesion and excludes normal tissues as much as possible (Xian et al., 2015). In this work, the ROI of each mammography is extracted by using PCNN to conduct coarsely segmentation. As illustrated in Figure 2, each pixel of the digitized mammography is corresponded to a neuron in the PCNN, and the gray-level values of the pixels are regarded as the inputs of the corresponding neurons, i.e., $S_{i,j} = G_{i,j}$, where $G_{i,j}$ denotes the gray-level value of the pixel (i,j) in original mammography. Then we initialize the PCNN by setting initial values to its parameters. This work uses an adaptive method, which was proposed in our previous work (Chen et al., 2011), to initialize the parameters for PCNN. After initialization, the neurons of PCNN are able to fire by iteration following (1)-(5). As a basic strength, PCNN is able to cause the adjacent neurons with similar inputs to pulse synchronously, resulting in great potential in image segmentation. Since we have corresponded pixels to PCNN neurons without changing their original locations, adjacent pixels with similar gray-level can be easily partitioned from the whole image by the procedure of synchronously firing. At the last iteration of PCNN, we should obtain a binary image. Each pixel of the binary image records whether its corresponding neuron has fired. The binary image is the result of the coarsely segmentation, i.e., ROI.

3.2 Defining Initial Contour for DRLSE

In this step, we use some simple yet effective geometric methods to define initial contour for DRLSE. As illustrated in Figure 3, the largest rectangle which is tangent to the foreground of the binary image is defined as the initial contour for DRLSE. Specifically, the foreground of the binary image denotes the largest close region in the image.

3.3 Finely Segmentation with DRLSE

Based on the results of preprocessing and coarsely segmentation (i.e., extraction of ROI), finely segmentation is achieved by DRLSE. To help the readers understand the process of evolution, Figure 4 visualizes the LSFs before and after evolution. Let's denote by $\phi_{i,j}^k$ the LSF with spatial index (i, j) and temporal index k. The LS evolution equation can be formulated by an iteration process as (Li et al., 2010)

$$\phi_{i,j}^{k+1} = \phi_{i,j}^k + \Delta t L\left(\phi_{i,j}^k\right), \quad k = 0, 1, 2, \cdots, \qquad (16)$$

where $L\left(\phi_{i,j}^k\right)$ denotes the approximation of the right hand side in the evolution equations, and is defined by

$$L\left(\phi_{i,j}^k\right) = \frac{\phi_{i,j}^{k+1} - \phi_{i,j}^k}{\Delta t}. \qquad (17)$$

In our implementation, the time-step Δt is fixed as $\Delta t = 5$, and the parameters in the DRLSE model, i.e., equation (15), are set as $\mu = 0.04$ and $\lambda = 5$, respectively. The value of α can be flexibly adjusted according to the contrast of the mammography.

4 EXPERIMENTAL RESULTS

4.1 Database and Settings

To provide a full spectrum of possible cases, the mammographies used in this work are taken from the Mammographic Image Analysis Society (MIAS) digital mammography database (Suckling et al., 1994), the digital database for screening mammography (DDSM) (Heath et al., 1998; Heath et al., 2001), and the mammography database of the Japanese Society of Medical Imaging Technology (JAMIT). The information of the three databases are summarized in Table 1.

As can be seen from Table 1, the patients of the three databases are from three different continents: Europe, America, and Asia, respectively. The MIAS

Table 1: Overview of the mammography databases.

Database	Provider	Continent
MIAS	Pilot European Image Processing Archive	Europe
DDSM	Department of Computer Science and Engineering, University of South Florida	America
JAMIT	Japanese Society of Medical Imaging Technology	Asia

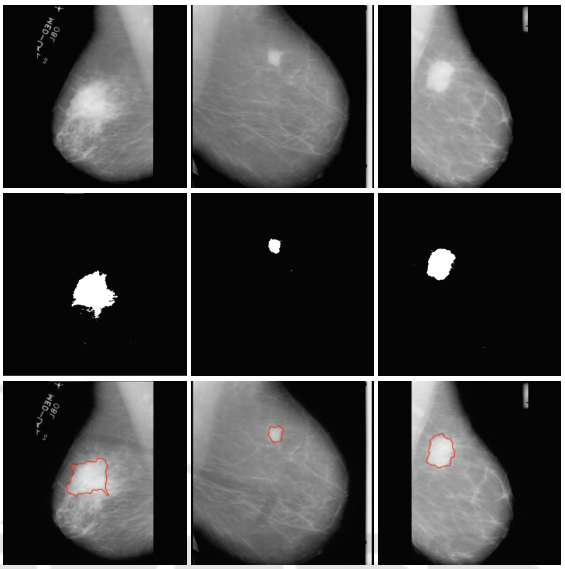

Figure 5: Typical segmentation results on MIAS database (corresponding patients are from Europe). In each column, from top to bottom: Original mammography, coarsely segmentation result from PCNN, and finely segmentation result from DRLSE.

digital mammography database contains 322 mammography screening exams which have been digitized to 50 micron per pixel with a linear optical density in the range 0-3.2, and each pixel is represented with an 8-bit word. The resolution of the images in MIAS database is 1024×1024 pixels. The images were annotated according to their corresponding types of abnormality by expert radiologists, using seven distinct classes: Calcification (23 images), well-defined/circumscribed mass (23 images), speculated mass (19 images), ill-defined mass (14 images), architectural distortion (19 images), asymmetry (15 images), and normal (209 images). The DDSM database contains 2620, four view, mammography screening exams. The mammography screening exams in DDSM database were digitized by one of four different scanners: DBA M2100 ImageClear (42 micron per pixel, 16 bit depth), HOWTEK 960 (43.5 micron per pixel, 12 bit depth), Lumisys 200 laser densitometer (50 micron per pixel, 12 bit depth), and HOWTEK MultiRAD 850 (43.5 micron per pixel, 12 bit depth) (Chen et al., 2015). The size of the images

in DDSM database varies, and the pathology types were annotated by expert radiologists as normal, cancer, benign, and benign without callback. The JAMIT mammography database contains 40 mammography screening exams which have been classified into three categories: normal (17 images), calcification (11 images), and tumor (12 images). Each of the mammography screening exams in the JAMIT mammography database was digitized to 2510×2000 pixels, and the bit-depth of each pixel is 10 (Arai et al., 2012). In this work, since the proposed approach focus on breast mass segmentation, only mammographies that contain a mass might be used for experiments. To bring the mammographies in DDSM and JAMIT databases into correspondence with those in MIAS database, they are resized to 1024×1024 pixels before segmentation. Following experiments are implemented by programming with the Mathworks Matlab 2010b on a PC with Intel Core-i5 processer and 4 GB RAM.

4.2 Experimental Results

Both subjective and objective evaluations on the performance of the proposed method are presented in this subsection. For European patients, Figure 5 presents several typical segmentation results of the proposed method on MIAS digital mammography database. By comparing the first row and the second row of Figure 5, we can see that the masses in the original mammographies are accurately positioned, and the rough shapes of the masses are also accurately contoured by PCNN. Besides, by examining the last row of Figure 5, we can find that the boundaries between masses and backgrounds are precisely positioned by DRLSE. For American and Asian patients, Figure 6 and Figure 7 present the typical segmentation results of the proposed method on DDSM and JAMIT mammography databases, respectively. The same conclusion can be drawn from Figure 6 and Figure 7. This is due to that the initial contour of DRLSE is adaptively defined in a mammography-specific way and DRLSE can ensure stable LS evolution.

The quantitative segmentation results of the proposed method and the ground-truth are listed in Table 2. In MIAS database, four mammographies, which contain circumscribed mass, asymmetry, ill-defined mass, and spiculated mass, respectively, were tested. In DDSM database, four mammographies, which contain masses with irregular shape, lobulated shape, and oval shape, were tested. In JAMIT database, four mammographies which contain tumors were also tested. The coarse and fine regions in Table 2 denote the coarsely and finely segmentation results of the proposed method, respectively. For each mammography, the MIAS mammography database provides us the coordinates of the centre of the abnormality and the approximate radius of a circle enclosing the abnormality. So the ground-truth regions of abnormalities in MIAS mammography database can be calculated with the coordinates and the radius. For DDSM mammography database, only thumbnail images which contain suspicious regions are available. So the ground-truth regions of abnormalities in DDSM mammography database can be approximately positioned with the thumbnail images. The fourth column of Table 2 lists the ground-truth, and the last two columns list the experimental results of the proposed algorithm. Comparing our results with ground-truth, we can find that, for every types of ab-

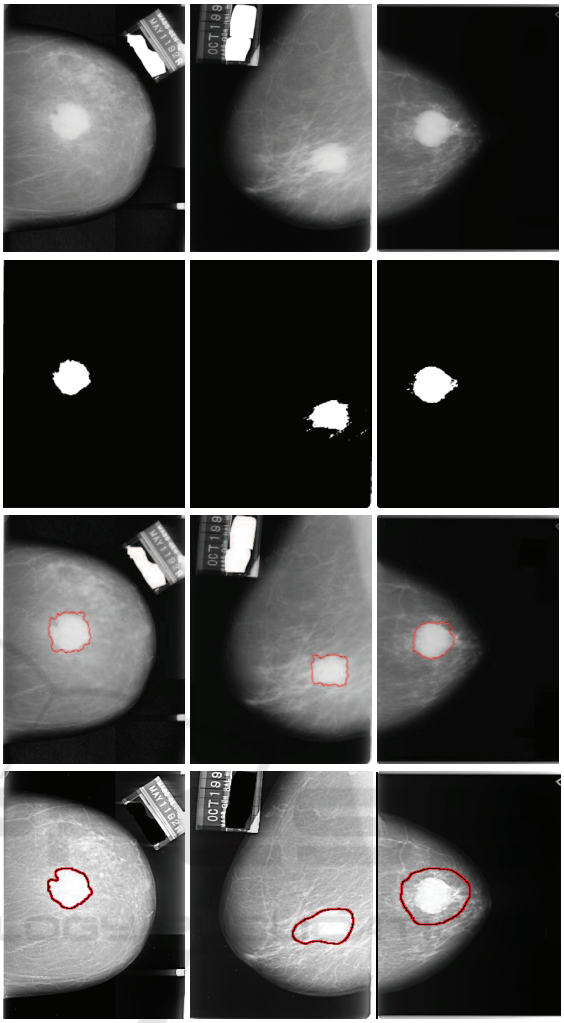

Figure 6: Typical segmentation results on DDSM database (corresponding patients are from America). In each column, from top to bottom: Original mammography, coarsely segmentation result from PCNN, finely segmentation result from DRLSE, and expert diagnosis (Heath et al., 1998; Heath et al., 2001).

Table 2: Performance of the proposed method.

Database	Mammography	Abnormality	Ground-Truth Region	Coarse Region	Fine Region
MIAS	mdb021	circumscribed mass	(444:542, 850:948)	(480:525, 880:915)	(428:580, 844:943)
	mdb081	asymmetry	(361:623, 420:682)	(420:560, 500:625)	(352:587, 426:635)
	mdb134	ill-defined mass	(420:518, 247:345)	(450:490, 273:328)	(433:516, 247:341)
	mdb202	spiculated mass	(520:594, 215:289)	(535:580, 235:275)	(510:596, 240:290)
DDSM	A_1004_1.RIGHT_CC	mass: irregular shape	(254:503, 399:566)	(278:495, 411:559)	(255: 492, 399:567)
	A_1006_1.LEFT_MLO	mass: irregular shape	(577:916, 566:713)	(657:901, 580:715)	(681:891, 575:705)
	C_0011_1.RIGHT_CC	mass: lobulated shape	(661:977, 565:745)	(711:878, 618:706)	(703:912, 567:719)
	C_0088_1.LEFT_CC	mass: oval shape	(128:515, 401:631)	(156:461, 438:592)	(199:432, 438:591)
JAMIT	T1	tumor	/	(517:676, 740:939)	(535:636, 711:845)
	T3	tumor	/	(412:490, 874:956)	(414:492, 882:966)
	T5	tumor	/	(528:596, 857:950)	(531:596, 868:935)
	T7	tumor	/	(508:609, 206:326) (429:565, 865:794)	(507:616, 185:328) (442:578, 629:783)

Noting that the positions of the mass regions were fixed after resizing.

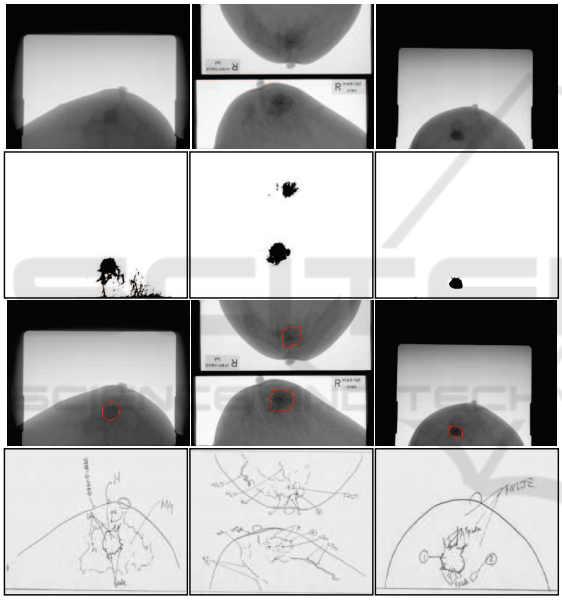

Figure 7: Typical segmentation results on JAMIT database (corresponding patients are from Asia). In each column, from top to bottom: Original mammography, coarsely segmentation result from PCNN, finely segmentation result from DRLSE, and expert diagnosis.

normalities, almost all of our results are inside the corresponding regions of ground-truth. This suggests that the proposed method encloses little normal tissues, proving the accuracy of our method.

5 CONCLUSION

We have presented a coarse-to-fine method for automatic breast mass segmentation in this paper. Specifically, PCNN is employed to fix the sketchy position of mass and extract ROI in the first step. The initial contour of DRLSE is then adaptively defined according to the position and the shape of the ROI. Finally, the precise boundary between mass and background is positioned with DRLSE. This is a novel and effective approach to partition mass in mammography for following reasons. First, ROI is extracted by PCNN in advance, which brings about a flexible and automatic definition of initial contour for DRLSE. Second, the DRLSE, which can ensure accurate computation and stable LS evolution, is firstly employed for the purpose of breast mass segmentation. Both subjective and objective experiments on three large-scale mammography databases prove that the ROI can be accurately fixed by PCNN, and the boundary between mass and normal tissue can be precisely positioned by DRLSE. In summary, the proposed method shows expectant segmentation performance.

On the other hand, considering its efficiency and accuracy, we expect that, in the future, the proposed breast mass segmentation algorithm will find its utility in more applications of medical image segmentation, such as vessel segmentation in fundus images and heart chamber segmentation in computed tomography (CT) images.

ACKNOWLEDGEMENTS

The authors would like to thank Dr. Chunming Li for shearing the source code of distance regularized level set evolution, and the members of the Institute of Circuits and Systems, School of Information Science and Engineering, Lanzhou University, for fruitful discussions and valuable advices. This work was supported by the National Natural Science Foundation of China (NSFC) under Grant 61175012, the Specialized Re-

search Fund for the Doctoral Program of Higher Education of China under Grant 20110211110026, and the Fundamental Research Funds for the Central Universities of China under Grant lzujbky-2015-196.

REFERENCES

Arai, K., Abdullah, I. N., and Okumura, H. (2012). Automated detection method for clustered microcalcification in mammogram image based on statistical textural features. *Int. J. Adv. Comput. Sci. Appl.*, 3(5):12–16.

Astley, S. M. (2004). Computer-based detection and prompting of mammographic abnormalities. *Br. J. Radiol.*, 45:S194–S200.

Chen, Y., Park, S. K., Ma, Y., and Ala, R. (2011). A new automatic parameter setting method of a simplified pcnn for image segmentation. *IEEE Trans. Neural Netw.*, 22(6):880–892.

Chen, Z., Strange, H., Oliver, A., Denton, E. R. E., Boggis, C., and Zwiggelaar, R. (2015). Topological modeling and classification of mammographic microcalcification clusters. *IEEE Trans. Biomed. Eng.*, 62(4):1203–1214.

Cui, Y., Tan, Y., Zhao, B., Liberman, L., Parbhu, R., Kaplan, J., Theodoulou, M., Hudis, C., and Schwartz, L. H. (2009). Malignant lesion segmentation in contrast-enhanced breast mr images based on the marker-controlled watershed. *Med. Phys.*, 36(10):4359–4369.

Du, S., Wu, G., Ma, L., and Ma, Y. (2014). Maximum quantum entropy based optimal threshold selecting criterion for thresholding image segmentation. *J. Comput. Inf. Syst.*, 10(8):3359–3366.

Eckhorn, R., Reitboeck, H. J., Arndt, M., and Dicke, P. (1989). Feature linking via stimulus-evoked oscillations: experimental results from cat visual cortex and functional implications from a network model. In *Proc. of the Int. Joint Conf. on Neural Networks*, pages 723–730.

Eckhorn, R., Reitboeck, H. J., Arndt, M., and Dicke, P. (1990). Feature linking via synchronization among distributed assemblies: Simulations of results from cat visual cortex. *Neural Comput.*, 2(3):293–307.

Eltonsy, N. H., Tourassi, G. D., and Elmaghraby, A. S. (2007). A concentric morphology model for the detection of masses in mammography. *IEEE Trans. Med. Imaging*, 26(6):880–889.

Estellers, V., Zosso, D., Lai, R., Osher, S., Thiran, J.-P., and Bresson, X. (2012). Efficient algorithm for level set method preserving distance function. *IEEE Trans. Image Process*, 21(12):4722–4734.

Guo, M., Dong, M., Wang, Z., Ma, Y., Guo, Y. (2015). A new method for mammographic mass segmentation based on parametric active contour model. In *Proc. of the Int. Conf. on Wavelet Analysis and Pattern Recognition*, pages 27–33.

Heath, M., Bowyer, K., Kopans, D., Kegelmeyer, W. P., Moore, R., Chang, K., and MunishKumaran, S. (1998). Current status of the digital database for screening mammography. In *Proc. of the Int. Workshop on Digital Mammography*, pages 457–460.

Heath, M., Bowyer, K., Kopans, D., Moore, R., and Kegelmeyer, W. P. (2001). The digital database for screening mammography. In *Proc. of the Int. Workshop on Digital Mammography*, pages 212–218.

Kuntimad, G. and Ranganath, H. S. (1999). Perfect image segmentation using pulse coupled neural networks. *IEEE Trans. Neural Netw.*, 10(3):591–598.

Li, C., Xu, C., Gui, C., and Fox, M. D. (2010). Distance regularized level set evolution and its application to image segmentation. *IEEE Trans. Image Process.*, 19(12):3243–3254.

Li, M., Cai, W., and Tan, Z. (2006). A region-based multisensor image fusion scheme using pulse-coupled neural network. *Pattern Recogn. Lett.*, 27(16):1948–1956.

Liang, X., Ramamohanarao, K., Frazer, H., and Yang, Q. (2012). Lesion segmentation in dynamic contrast enhanced mri of breast. In *Proc. of the Int. Conf. on Digital Image Computing Techniques and Applications*, pages 1–8.

Moraru, L., Moldovanu, S., and Biswas, A. (2014). Optimization of breast lesion segmentation in texture feature space approach. *Med. Eng. Phys.*, 36(1):129–135.

Osher, S. and Sethian, J. A. (1988). Fronts propagating with curvature-dependent speed: Algorithms based on hamilton-jacobi formulations. *J. Comput. Phys.*, 79(1):12–49.

Rouhi, R., Jafari, M., Kasaei, S., and Keshavarzian, P. (2015). Benign and malignant breast tumors classification based on region growing and cnn segmentation. *Expert Syst. Appl.*, 42(3):990–1002.

Suckling, J., Parker, J., Dance, D. R., Astely, S., Hutt, I., Boggis, C. R. M., Ricketts, I., Stamatakis, E., Cerneaz, N., Kok, S.-L., Taylor, P., Betal, D., and Savage, J. (1994). The mammographic image analysis society digital mammogram database. In *Proc. of the Int. Congress Series on Exerpta Medica*, pages 375–378.

Wang, Z., Ma, Y., Cheng, F., , and Yang, L. (2010). Review of pulse-coupled neural networks. *Image and Vision Comput.*, 28(1):5–13.

Wang, Z., Yu, G., Kang, Y., Zhao, Y., and Qu, Q. (2014). Breast tumor detection in digital mammography based on extreme learning machine. *Neurocomputing*, 128:175–184.

Xian, M., Zhang, Y., and Cheng, H. D. (2015). Fully automatic segmentation of breast ultrasound images based on breast characteristics in space and frequency domains. *Pattern Recognit.*, 48(2):485–497.

Xie, W., Ma, Y., and Li, Y. (2015). Breast mass segmentation in digital mammography based on pulse coupled neural network and level set method. In *Proc. of the Satellite Data Compression, Communications, and Processing XI*, page 95010J.

Xie, W., Li, Y., and Ma, Y. (2016). Breast mass classification in digital mammography based on extreme learning machine. *Neurocomputing*, 173:930–941.

Zhang, L. and Ji, Q. (2011). A bayesian network model for automatic and interactive image segmentation. *IEEE Trans. Image Process.*, 20(9):2582–2593.

Zhou, L., Sun, Y., and Zheng, J. (2008). Automated color image edge detection using improved pcnn model. *WSEAS Trans. Computers*, 7(4):184–189.